International Scholarly Research Network
ISRN Ceramics
Volume 2012, Article ID 972054, 6 pages
doi:10.5402/2012/972054

Research Article

Microstructural Modeling of Ni-Al_2O_3 Composites Using Object-Oriented Finite-Element Method

Neeraj Kumar Sharma,[1] S. N. Pandit,[1] and Rahul Vaish[2]

[1] *Noida Institute of Engineering and Technology, Greater Noida 201306, India*
[2] *School of Engineering, Indian Institute of Technology Mandi, Mandi 175 001, India*

Correspondence should be addressed to Rahul Vaish, rahul@iitmandi.ac.in

Received 31 July 2012; Accepted 6 September 2012

Academic Editors: K. Oh-Ishi and W.-H. Tuan

This paper studied the mechanical and thermal properties of interpenetrating phase composites (IPCs) of Ni-Al_2O_3 using finite-element-based object-oriented program (OOFEM). It is difficult to model structure-property relationship in IPCs because of interpenetration of two or more phases. In order to understand the material behavior, OOFEM combines the microstructural data in the form microscopic images with the fundamental material properties (such as Young's modulus or thermal conductivity of the constituent phases). Thermal conductivity, thermal expansion coefficient, and modulus of elasticity for the composites are examined using OOFEM and compared with other methods. The distribution of residual thermal stresses is also investigated.

1. Introduction

The recent advances in composite science and technology have resulted in the design of microstructures for specific purposes. In order to achieve the improved properties, the focus is gradually shifted from traditional composite materials with discrete, dispersed additions to incorporating larger quantities of reinforced material or utilizing the processing routes that result in composites with a connected reinforced phase. Interpenetrating phase composites (IPCs) are such new class of composites and have attracted much attention over the past decade. In IPCs, both the phases span throughout the microstructure and from 3D networks interpenetrating each other [1]. Many researchers have reported the processing and physical properties of metal/ceramic IPCs [2–6]. Ceramic-metal composites have great potential in various technological fields due to their improved thermal, mechanical and electrical properties.

The present study is concerned with analyzing the thermal and mechanical behavior of Ni-Al_2O_3 composites (IPCs) using finite-element method. There are different modeling approaches used by many researchers to describe the mechanical and thermal behavior of Ni-Al_2O_3 composites [7, 8]. These approaches are mainly macroscopic in nature. The most of the macroscopic models do not consider particle size, shape, and orientation. Situation is more complicated in case of IPCs. Hence it is difficult to predict/validate physical properties of interpenetrating composites. Various rules of mixtures (ROMs) formulation are reported for assessing properties of composites. In order to have a better agreement with experimental observations, the ROM formulation has been modified for considering various physical factors. Variety of analytical models have been proposed for analyzing the metal-ceramic composites [9–12]. In this paper, an attempt is made to study mechanical/thermal properties of Ni-Al_2O_3 composites with the OOFEM and compared their results with that of other models. OOFEM technique has been applied for various composite/heterogeneous materials [13, 14] using open source software (OOF2) which is available at National institute of standards and technology, USA website. Many unique and special features of OOF2 software make it an effective tool for the image-based material analysis [15, 16].

2. Materials and Methods

In interpenetrating phase composites (IPCs) both phases are three-dimensionally (3D) continuous. The advantage

with such interpenetrating microstructures is that they offer improved and unique combinations of mechanical and thermal properties. Experimental investigation on nickel/alumina composites has been reported [8]. Authors have been producing composites of various volume fractions of nickel and alumina using hot-pressing method. Microstructural details are reported for five different samples of Ni (15%, 35%, 50%, 65%, and 85%)-Al_2O_3 composites [8]. The present OOFEM analysis is performed on the scanning electron microscopic images of these composites.

2.1. Microstructural Simulation Using OOF2. Finite element program (OOF2) has been extensively used to investigate the microstructure-property correlation in wide range of materials. This program is based on microstructural images which can be collected using optical or electron microscopes. Various tools for image segmentation including median filters, edge detection, blurring filters which can be employed based on the nature of image. Materials properties need to be assigning after image segmentation. A number of mechanical, thermal, and electric properties is included in the latest version of OOF2 [15]. Figure 1 shows a typical processed scanning electron microscopic image of nickel/alumina composite.

2.2. Mesh Generation and Refinement. Once the material properties of each phase are assigned, the next step is the mesh generation of the microstructure. Mesh generation in OOF2 can be done only after creating a skeleton. The skeleton defines basically the geometry of a finite element mesh by specifying the node positions and element edges only. It does not create any information about the finite element interpolation functions or the fields to be defined. The skeleton modification tools allow us to adapt the skeleton to the geometry of microstructure. A microstructure can contain more than one skeleton. In OOF2, the skeleton is a regular array of triangular or quadrangular elements. This mesh is adapted to the microstructure by an "adaptive meshing" procedure, which allows subdivision of the elements and movement of the nodes to conform to the microstructure. Split quadrangular, refine and snap refine are some of the tools used for subdivision of the elements while anneal, snap nodes & snap anneal are used for the node movement [16]. Skeletons are effective if each of its elements are homogeneous (area consists of only one type of pixel group in the microstructure). This procedure involves the minimization of an energy functional parameter of the mesh, E. There are two components to the energy function, a shape component, E_{shape}, and a homogeneity component, E_{hom}. The contribution to E_{shape} for an element is a minimum when the triangular element is equilateral or when a quadrangular element is square as shown in Figure 2. Thus, the deviation of the triangular element from equilateral triangle shape increases the E_{shape} component. In order to minimize the contribution to E_{hom} for an element, the mesh has to be refined in such a way that each element encompasses only a single phase.

The total energy functional parameter, E, can then be computed as the sum of the two energy terms described for each mesh element:

$$E = \alpha E_{\text{hom}} + (1 - \alpha) E_{\text{shape}}, \tag{1}$$

where the parameter α has value between 0 and 1, and E_{hom} and E_{shape} are the functions that depend on the element's homogeneity and shape, respectively. While refining a mesh if α has assigned a value equal to zero, then the resulting mesh will have square or equilateral triangular elements (providing good finite-element convergence) but their positions may not quite correspond to the nature of the material microstructure. It is always better to first focus upon the minimization of E_{hom} component by assigning higher value of α. The homogeneity index for the skeleton is displayed on the screen after each mesh refinement step. Once the homogeneity aspect of mesh is realized the next step is to improve the shape of the elements. There are tools like rationalize, swap edges, merge triangles, and smooth which can improve the quality of meshing. Finite element mesh can be created from a skeleton. The single skeleton can have many meshes. In each mesh, one mesh element is created for each skeleton element, and one mesh node is created for each skeleton vertex. OOF2 currently supports three- and six-nodded triangular elements and four-, eight-, and nine-nodded quadrilateral elements.

2.3. Boundary Conditions and Simulation. After creating a mesh, the next step is the activation of fields. OOF2 can solve problems for displacement, temperature, and voltage fields. The characteristics which are computed as secondary characteristics are not considered as field in OOF2. For example, heat flux is a field in the sense that it has values everywhere in the continuum, but in OOF2, it is computed as secondary characteristic and not as a fundamental quantity hence it is not considered as a field in OOF2 software. Divergence equations and plane-flux equations are the two types of equations that OOF2 can solve. OOF2 supports five kinds of boundary conditions: Dirichlet, Neumann, floating, generalized force, and periodic. Once the boundary conditions are defined, in the next step we can solve and analyze the field and fluxes. Figure 3 shows the deformed mesh under Dirichlet boundry condition for the applied displacement.

3. Results and Discussion

3.1. Mechanical Behavior of Ni-Alumina Composites. The microstructures of the Ni-Alumina composites were examined by scanning electron microscope (SEM) [8] and these images are used for analysis in OOF2 program. The material properties used in present analysis are mentioned in Table 1. All the samples were analyzed under same boundry conditions (Dirichlet boundary condition, u_x= 10 at right side, u_y = 0 at left side, u_y = 0 at bottom). Elastic modulus is studied using OOF2, rule-of-mixtures approach, and Hashin-Shtrikman analytical bounds [9], for Ni/Alumina composites, and are presented in Figure 4.

The value obtained using OOF2 are slightly higher than other methods under studied. The calculation for Young's modulus from rule-of-mixtures is based on the assumption of isostrain between the constituents of the composite, that is, there is a perfect bonding between the constituents. This assumption reduces the longitudinal strain and hence Young's modulus obtained from rule-of-mixtures is higher than that of OOF2 & Hashin's bounds. Further, Hashin and Shtrikman [9] proposed upper and lower bounds for an isotropic aggregate based on variational principles of linear elasticity as follows:

$$K_{\text{upper}} = K_p + \left(1 - V_p\right)\left[\frac{1}{\left(K_m - K_p\right)} + \frac{3V_p}{\left(3K_p + 4G_p\right)}\right]^{-1}, \quad (2a)$$

$$K_{\text{lower}} = K_m + V_p\left[\frac{1}{\left(K_p - K_m\right)} + \frac{3\left(1 - V_p\right)}{(3K_m + 4G_m)}\right]^{-1}, \quad (2b)$$

$$G_{\text{upper}} = G_p + \left(1 - V_p\right)\left[\frac{1}{\left(G_m - G_p\right)} + \frac{6V_p\left(K_p + 2G_p\right)}{5G_p\left(3K_p + 4G_p\right)}\right]^{-1}, \quad (2c)$$

$$G_{\text{lower}} = G_m + V_p\left[\frac{1}{\left(G_p - G_m\right)} + \frac{6\left(1 - V_p\right)(K_m + 2G_m)}{5G_m(3K_m + 4G_m)}\right]^{-1}, \quad (2d)$$

where G and K are the shear and bulk modulus, respectively. V_p is the volume fraction of reinforcement (filler). m and p subscript denote matrix and filler. The subscripts "upper" and "lower" refer to the upper and lower bound estimates, respectively. Substituting the modulus values of matrix and reinforcement, the overall bounds of Young's modulus can be obtained by the following equation:

$$E = \frac{9KG}{(G + 3K)}. \quad (3)$$

The OOF2 data fall reasonably between the upper and lower bounds of the Hashin–Shtrikman model for composites having volume fraction of nickel less than 0.65. For 0.65 and 0.85 nickel reinforced composites, the OOF2 prediction of elastic modulus is slightly higher than the upper bond of Hashin-Shtrikman model. For 0.65 & 0.85 samples, OOF2 predicts 2% higher values than that of upper bound of Hashin-Shtrikman model.

In order to further study, local stress distribution in the composites is also investigated that could be helpful to understand microstructural behavior of these composites. The stress distribution for 0.35 (35%) Ni sample is depicted in Figure 5. The intensification of stress can be observed in the clustered region. Regions where particles touch are also sites of high stress concentration especially if there are some sharp corners, as it is being shown in Figure 5, and thus these sites are more prone for crack initiation. The stress contour for σ_{xx} component is shown in Figure 6 for 35% nickel-reinforced composites. The heterogeneous stress distribution is depicted. The yellow & saffron colored region shows the high stresses in the range of 9 GPa to 11.7 GPa, in alumina elements while the maroon-colored region is stressed in the range of 5.12 GPa to 6.39 GPa in nickel elements.

Table 1: Properties of nickel and alumina.

Material properties	Nickel	Alumina
Young's modulus (GPa)	200	375
Poisson's ratio	0.31	0.22
Thermal-conductivity (w/mK)	90.9	35
Thermal expansion coefficient (C^{-1})	$13.4 * 10^{-6}$	$8.4 * 10^{-6}$

Figure 7 shows the stresses induced in different samples when all samples are subjected to same boundary conditions and a comparison is made with pure alumina sample. For 15%, 35%, 50%, 65% and 85% samples, the stresses induced under same boundary conditions are 12.3%, 21.2%, 27.8%, 31.9%, and 39.7% lower, respectively, than that of the stress induced in pure alumina. The nickel reinforcement in alumina significantly reduces the residual stresses in the composites.

3.2. Thermal Behavior of Ni-Alumina Composites

3.2.1. Thermal Conductivity Behavior. In this section, thermal behavior of the composite is studied using OOF2. This study includes the measurement of the thermal conductivity of the composites using OOF2 at 50°C and comparing the same with the rule-of-mixtures. Thermal conductivity of the composites has been studied using OOF2 [13]. While working with OOF2, the fixed temperature boundary conditions (100°C temperature at right side & 0°C at left side boundary) are applied to the boundary of the mesh so that the average temperature is 50°C and steady state heat transfer condition can be assumed. The comparison of thermal conductivities calculated using OOF2 and ROM are shown in Figure 8.

Thermal conductivity of the composites increases due to the reinforcement of highly conductive nickel particles in the alumina matrix. The difference between the effective thermal conductivity estimated using OOF2 & rule-of-mixture is within the range of 2%, except in the case of 65% sample where the OOF2 predicts 4.4% lower value. Thermal conductivity calculation using ROM is based on "zero thermal contact resistance" between the constituents. If there is not a perfect contact between the constituents than the prediction from ROM cannot be accurate. In present study since the material is not porous hence there is marginal difference between OOF2 & ROM results. The slight mismatch between the results of OOF2 and ROM

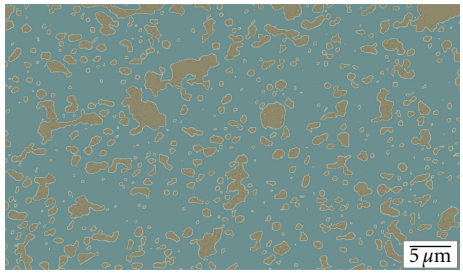

Figure 1: A typical image for 15% nickel/alumina composites.

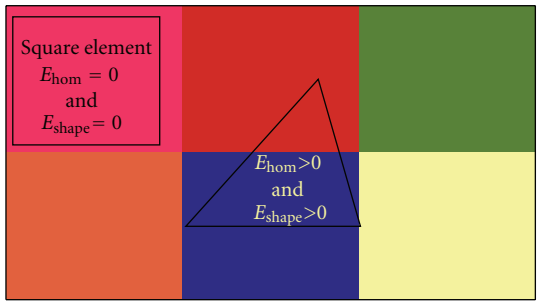

Figure 2: E_{hom} and E_{shape} for square and triangular elements during mesh generation.

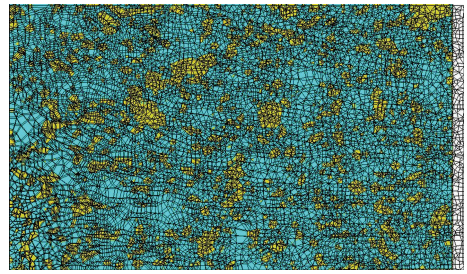

Figure 3: Mesh deformation due to displacement based on Dirichlet boundary condition.

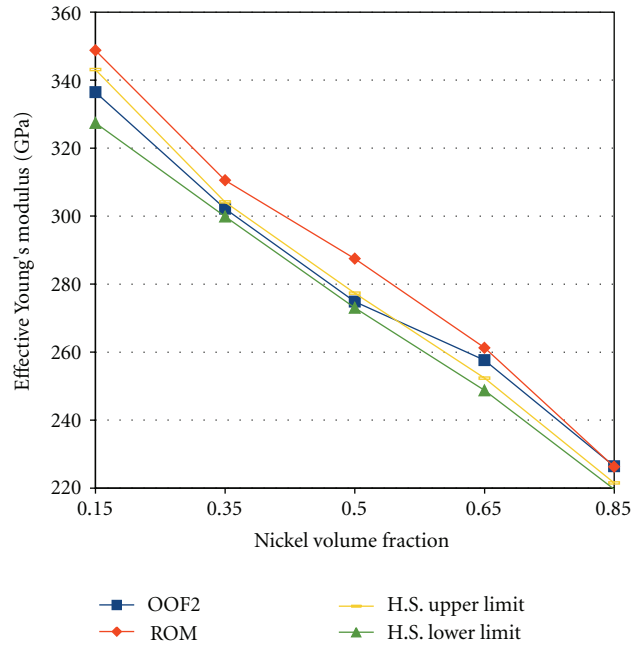

Figure 4: Elastic modulus estimated using OOF2, ROM & Hasin-Shtrikman's upper and lower bounds.

can be attributed to the fact that there is no consideration of distribution and shape of reinforced particles in ROM formulation and it predicts the average thermal conductivity based on the volume fractions and individual properties of the constituents. Heat flux (XX component) distribution across the mesh is also shown in Figure 9. The yellow elements (shown in the contour) show the heat flux across the alumina. It is because $k_{\text{Alumina}} < k_{\text{nickel}}$, the heat flow preferably through the nickel region as can be seen from the distribution of heat flux where red and orange elements shows the heat flux across the nickel.

3.2.2. Thermal Expansion Behavior. Nickel-alumina composites have great potential in various high temperature applications hence it would be interesting to study the thermal expansion coefficient for these composites. Thermal expansion behavior of metal-ceramic composites is studied in detail earlier also [17–19]. In this section, the coefficient of thermal expansion is evaluated by using OOF2 and different analytical models. The predictions from the analytical models [10–12] and the OOF2 model are compared. Analytical solutions proposed by Turner [10] and Schapery [12] are used to evaluate the thermal expansion coefficient of particulate composites. Since we are working with two-dimensional model, we use the coefficient of linear expansion. According to Turner [10]

$$\alpha_C = \frac{\left(\alpha_m K_m V_m + \alpha_p K_p V_p\right)}{\left(K_m V_m + K_p V_p\right)}, \tag{4}$$

where α is the linear coefficient of thermal expansion, volume fraction is V, bulk modulus is K, and the subscripts c, m, and p denote the composite, matrix, and reinforcement, respectively.

The upper and lower bounds of the linear thermal expansion coefficient were given by Schapery [12] as follows:

$$\alpha_C = \alpha_m V_m + \alpha_p V_p + \left[\frac{4G_m}{K_c}\right]\left[\frac{\left(K_c - K_p\right)\left(\alpha_m - \alpha_p\right)V_p}{\left(4G_m + 3K_p\right)}\right], \tag{5}$$

where K_c is the bulk modulus of the composite as evaluated in case of Hashin and Shtrikman bounds. Here we consider K_c as the average of the upper and lower bounds, K_{upper} and K_{lower} of the bulk modulus, for our analysis. The lower bound

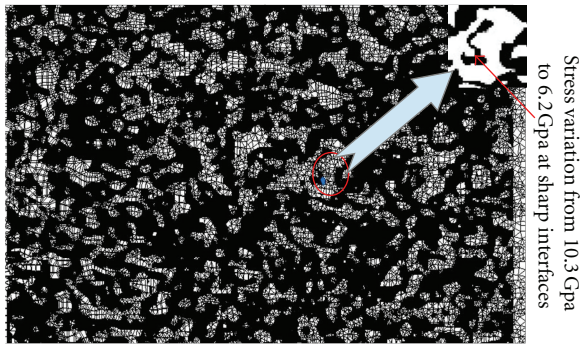

Figure 5: Microstructure for 35% Ni-Al_2O_3 composites depicting the sharp variation in stress (σ_{xx} component) at Ni-Alumina interfaces.

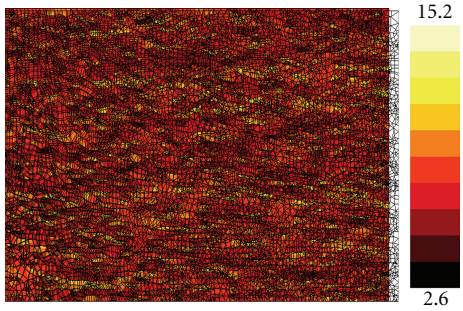

Figure 6: Stress (σ_{xx} component) contour for 35% sample.

given by Schapery [12] is same as (5), with interchange of subscripts p and m as follows:

$$\alpha_C = \alpha_m V_m + \alpha_p V_p + \left[\frac{4G_p}{K_c}\right]\left[\frac{(K_c - K_m)(\alpha_p - \alpha_m)V_m}{(4G_p + 3K_m)}\right]. \quad (6)$$

The OOF2 prediction of thermal expansion coefficient differs slightly from the analytical models. ROM-predicted values for the coefficient of thermal expansion is closest to values predicted by OOF2 (Figure 10). The mismatch between the predictions obtained from the rule-of-mixtures and OOF2 decreases as the concentration of nickel increases. For 85% and 65% reinforced nickel, the OOF2 predicts approximately 1% higher values, for 50% and 35% samples OOF2 predicts approximately 3% higher values while for 15% samples OOF2 predicts 5% higher value of coefficient of thermal expansion than that of predicted by ROM methods. Rule of mixture predicts lower values of thermal expansion coefficient. It is due to the assumption of isostrain between the matrix and reinforcement that lowers the longitudinal strain and hence the predicted thermal expansion coefficient for the composite is lower.

4. Conclusions

An attempt has been made to study Ni-Al_2O_3 interpenetrating composites using the finite element analysis in order to study their mechanical and thermal properties. A comparison of physical properties estimated from various analytical models and OOF2 shows that OOF2 is an effective tool for evaluating material behavior under thermal and/or mechanical conditions, because it incorporates the actual microstructure of the material (including distribution, shape and size of particles). It is found that the rule-of-mixtures over predict the values of modulus of elasticity due to the isostrain assumption between the constituents while OOF2 prediction for 15%, 35%, and 50% nickel-reinforced composites lies between the upper and lower bond of Hashin & Shtrikman values and for 65% and 85% samples OOF2 prediction differs slightly. Thermal conductivity predicted using OOF2 differs from that of rule-of-mixture's predictions within the range of 2%, except for the 65% nickel reinforced sample, where OOF2 predicts 4.4% lower value than that estimated using ROM methods. OOF2 results are more efficient and reliable than that of rule of mixture which

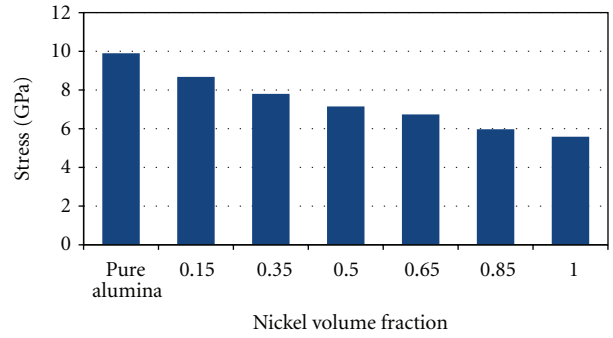

Figure 7: Average stress (σ_{xx}) induced in various samples under similar boundary conditions.

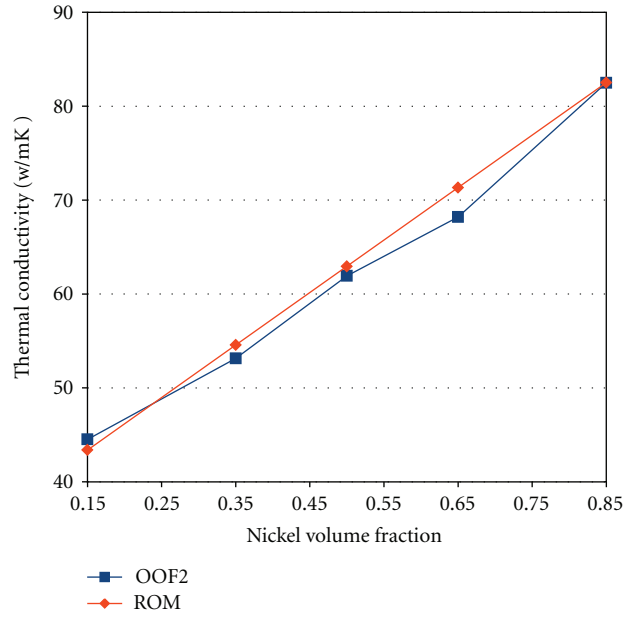

Figure 8: Comparison of thermal conductivities calculated using OOF2 and rule-of-mixtures.

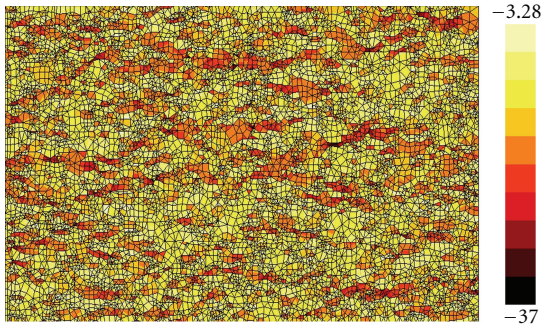

Figure 9: Heat flux (x component) distribution in the 35% nickel reinforced composites.

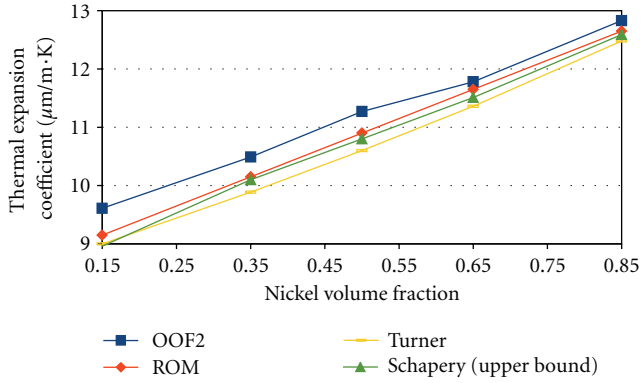

Figure 10: Coefficient of thermal expansion estimated from rule-of-mixtures, Turner, Schapery, and OOF2 models.

merely predicts on the basis of respective volume fractions and individual properties of constituents. OOF2 is used to assess the local stress distributions in the microstructure.

Acknowledgments

R. Vaish acknowledges support from the Indian National Science Academy (INSA), New Delhi, through a grant by the Department of Science and Technology, (DST), New Delhi, under INSPIRE faculty award-2011 (ENG-01). N. K. Sharma gratefully acknowledges Prof. S.A. Langer for his valuable suggestions.

References

[1] D. R. Clarke, "Interpenetrating phase composites," *Journal of the American Ceramic Society*, vol. 75, pp. 739–759, 1992.

[2] M. K. Aghajanian, N. H. MacMillan, C. R. Kennedy, S. J. Luszcz, and R. Roy, "Properties and microstructures of Lanxide Al_2O_3-Al ceramic composite materials," *Journal of Materials Science*, vol. 24, no. 2, pp. 658–670, 1989.

[3] H. Prielipp, M. Knechtel, N. Claussen et al., "Strength and fracture toughness of aluminum/alumina composites with interpenetrating networks," *Materials Science and Engineering A*, vol. 197, no. 1, pp. 19–30, 1995.

[4] W. Liu and U. Köster, "Microstructures and properties of interpenetrating alumina/aluminium composites made by reaction of SiO_2 glass preforms with molten aluminium," *Materials Science and Engineering A*, vol. 210, no. 1-2, pp. 1–7, 1996.

[5] R. E. Loehman, K. Ewsuk, and A. P. Tomsia, "Synthesis of Al_2O_3-Al composites by reactive metal penetration," *Journal of the American Ceramic Society*, vol. 79, no. 1, pp. 27–32, 1996.

[6] W. G. Fahrenholtz, D. T. Ellerby, and R. E. Loehman, "Al_2O_3-Ni composites with high strength and fracture toughness," *Journal of the American Ceramic Society*, vol. 83, no. 5, pp. 1279–1280, 2000.

[7] H. A. Bruck and B. H. Rabin, "Evaluating microstructural and damage effects in rule-of-mixtures predictions of the mechanical properties of Ni-Al_2O_3 composites," *Journal of Materials Science*, vol. 34, no. 9, pp. 2241–2251, 1999.

[8] D. E. Aldrich and Z. Fan, "Microstructural characterisation of interpenetrating nickel/alumina composites," *Materials Characterization*, vol. 47, no. 3-4, pp. 167–173, 2001.

[9] Z. Hashin and S. Shtrikman, "A variational approach to the theory of the elastic behaviour of multiphase materials," *Journal of the Mechanics and Physics of Solids*, vol. 11, no. 2, pp. 127–140, 1963.

[10] P. S. Turner, "Thermal-expansion stresses in reinforced plastics," *Journal of Research of the National Bureau of Standards*, vol. 37, p. 239, 1946.

[11] E. H. Kerner, "The elastic and Thermo-elastic properties of composite media," *Proceedings of the Physical Society B*, vol. 69, no. 8, pp. 808–813, 1956.

[12] R. A. Schapery, "Thermal expansion coefficients of composite materials based on energy principles," *Journal of Composite Materials*, vol. 2, no. 3, pp. 380–404, 1968.

[13] S. R. Bakshi, R. R. Patel, and A. Agarwal, "Thermal conductivity of carbon nanotube reinforced aluminum composites: a multi-scale study using object oriented finite element method," *Computational Materials Science*, vol. 50, no. 2, pp. 419–428, 2010.

[14] N. Chawla, B. V. Patel, M. Koopman et al., "Microstructure-based simulation of thermomechanical behavior of composite materials by object-oriented finite element analysis," *Materials Characterization*, vol. 49, no. 5, pp. 395–407, 2002.

[15] A. C. E. Reid, R. C. Lua, R. E. García, V. R. Coffman, and S. A. Langer, "Modelling microstructures with OOF2," *International Journal of Materials and Product Technology*, vol. 35, no. 3-4, pp. 361–373, 2009.

[16] A. C. E. Reid, S. A. Langer, R. C. Lua, V. R. Coffman, S. I. I. I. Haan, and R. E. García, "Image-based finite element mesh construction for material microstructures," *Computational Materials Science*, vol. 43, no. 4, pp. 989–999, 2008.

[17] S. Elomari, R. Boukhili, and D. J. Lloyd, "Thermal expansion studies of prestrained $A1_2O_3$/A1 metal matrix composite," *Acta Materialia*, vol. 44, no. 5, pp. 1873–1882, 1996.

[18] Y.-L. Shen, A. Needleman, and S. Suresh, "Coefficients of thermal expansion of metal-matrix composites for electronic packaging," *Metallurgical Transactions A*, vol. 25, no. 4, pp. 839–850, 1994.

[19] M. Olsson, A. E. Giannakopoulos, and S. Suresh, "Elastoplastic analysis of thermal cycling: ceramic particles in a metallic matrix," *Journal of the Mechanics and Physics of Solids*, vol. 43, no. 10, pp. 1639–1671, 1995.